Comparison of ADCP observations and 3D model simulations of turbulence at a tidal energy site

Michael Togneri [a, *], Matt Lewis [b], Simon Neill [b], Ian Masters [a]

[a] College of Engineering, Swansea University, Bay Campus, Swansea, SA1 8EN, UK
[b] School of Ocean Sciences, Bangor University, Menai Bridge, LL59 5AB, UK

A B S T R A C T

Field measurement of turbulence in strong tidal currents is difficult and expensive, but the tidal energy industry needs to accurately quantify turbulence for adequate resource characterisation and device design. Models that can predict such turbulence could reduce measurement costs. We compare a Regional Ocean Modelling System (ROMS) simulation with acoustic Doppler current profiler (ADCP) measurements from a highly-energetic tidal site. This comparison shows the extent to which turbulence can be quantified by ROMS, using the conventional $k - \varepsilon$ turbulence closure model. Both model and observations covered the same time period, encompassing two spring-neap cycles. Turbulent kinetic energy (TKE) density was calculated from measurements using the variance method; turbulent dissipation, ε, was calculated using the structure function method. Measurements show that wave action dominates turbulent fluctuations in the upper half of the water column; comparing results for deeper water, however, shows very strong agreement. A best fit between ROMS and ADCP results for mean velocity yields $R^2 = 0.98$; for TKE, R^2 is 0.84 when strongly wave-dominated times are excluded. Dissipation agrees less well: although time series of ε are well-correlated at similar depths, ROMS estimates a greater magnitude of dissipation than is measured, by a factor of up to 4.8.

1. Introduction

Tidal energy converters (TECs) generate electricity from tidal currents, with most designs using similar physical principles to conventional wind turbines. However, the marine environment in which they are deployed and operate poses its own set of technical hurdles that must be addressed [1—3]. Turbulence in tidal currents, which differs from atmospheric turbulence, is one of these challenges, and an important one for the development of TECs due to its impact on loading, reliability and fatigue life [4,5]. Oceanographic modelling of turbulence has generally focussed on vertical mixing for transport of sediments or nutrients [6,7] rather than the highly-energetic turbulence typical of sites with strong tidal currents that are likely candidates for TEC deployment. In this paper, we present a comparison of turbulence measurements from such a site to estimates from a basin-scale numerical model. Deploying, operating and retrieving instrumentation suitable for turbulence measurements in marine currents is an expensive and time-consuming

process, but the highly site-specific nature of marine turbulence means such measurements are vital to understanding turbulence in tidal currents. If it can be shown, by comparison with measured data, that oceanographic modelling can predict turbulence with some accuracy, then such models can be used to aid in targeting measurement campaigns at the most beneficial sites and times. Confidence in oceanographic models' ability to estimate turbulence at TEC deployment candidate sites will also mean that its predictions would be suitable for defining the inflow conditions of smaller-scale models of TEC arrays or even individual devices [8,9].

The site for this study is the West Anglesey Demonstration Zone (WADZ) off the coast of Wales, which has been designated for the development of tidal power by the Crown Estate. Measurements were taken with an RDI Sentinel V acoustic Doppler current profiler (ADCP) deployed on the edge of the WADZ between the 19th of September and the 19th of November 2014. A wave buoy measuring significant wave height and period was simultaneously deployed approximately 2 km to the south of the ADCP. The bathymetry of the site, and the location of the ADCP and buoy, are shown in Fig. 1. Water depth at the ADCP's location varied between 41.1 and 46.2 m through the deployment period, giving a spring range of around 5 m, and peak depth-averaged spring currents were 2.5 ms^{-1}. There

was a blanking distance of 1.89 m between the first bin and the transducer head, and subsequent bins had a vertical separation of 0.6 m. A 15-min burst of data was collected every hour; during the burst, the measurements were taken at a rate of 2 Hz. The ping frequency was 614.4 kHz.

The tidal hydrodynamics were simulated using the 3D Regional Ocean Modelling System (ROMS), which uses finite-difference approximations of the Reynolds-Averaged Navier-Stokes equations with hydrostatic and Boussinesq assumptions [10–12], and is regularly used in tidal-stream energy resource studies [13–15]. Turbulence is modelled in ROMS by a two-equation scheme. The first equation is for the transport of turbulent kinetic energy (TKE), k; the second equation represents a generic length scale (GLS) that can be tuned to a variety of standard turbulence models [16]. For this study, the well-established $k - \varepsilon$ model was implemented.

A comparison of turbulence parameters from a ROMS model and field measurements in Puget Sound in the USA has been previously carried out by Thyng et al. [17]. Although some ADCP data was in their study, most of the validation was done using single-point, high-frequency acoustic Doppler velocimeter measurements. Furthermore, the study presented here uses a much larger dataset, covering approximately two months as opposed to two days; this allows us to compare the long-term turbulence dynamics of the ROMS model to real measurements and to demonstrate that the numerical estimates adequately capture the range of turbulent conditions observed with instruments.

2. Methods

2.1. Turbulence measurement using ADCPs

ADCPs are a widely-used tool for the measurement of marine currents. By measuring the Doppler shift in the backscattered signals from an array of acoustic beams, they are able to measure three-dimensional velocities [18–20]. Since their initial deployment, new techniques of analysing the data they gather has allowed researchers to measure not only the mean flow currents but also their turbulent properties.

It is possible to calculate a range of turbulence parameters using a variety of methods. The variance method is a standard technique for estimating TKE density and Reynolds stresses [21,22], and dissipation can be estimated by structure function analysis [23] or spectral analysis [24]. Time- and lengthscales can be estimated from the time-lagged autocorrelation of the beam measurements [25]. The use of ADCPs for surveying turbulence at planned or current tidal stream deployment sites is a well-established method, both used alone [26–29] or in combination with other techniques and instrumentation [30,31].

2.1.1. Turbulent kinetic energy

TKE, or more precisely TKE density, is a measure of the energy contained in turbulent fluctuations per kilogram of fluid. If we denote the fluctuation velocity measured by each beam with b_i', we can relate the TKE to the beam variances as follows:

$$k = \frac{\sum_{i=1}^{4} \left\langle b_i'^2 \right\rangle}{4 \sin^2 \theta (1 - \xi(1 - \cot^2 \theta))}, \tag{1}$$

where the summation is over the four off-vertical beams, ξ is a parameter that characterises the anisotropy of the flow, and θ is the inclination angle of the beams. Following the work of Nezu and Nakagawa [32], we set ξ to 0.1684.

This formulation assumes that the device accurately measures the true velocity in the fluid. In reality, instrument noise will introduce an error between the true and measured along-beam velocities. This instrument noise can be regarded as a normally distributed, zero-mean random error. For calculation of mean velocities, the time-averaging process means that no bias is introduced, as the noise is zero-mean. However, in calculating the variance the instrument noise becomes more significant. If we write the fluctuation velocity measured by the ith beam, b_i', as the sum of a true fluid velocity β_i' and Gaussian noise N, then we find that:

$$\text{Var}(b_i') = \text{Var}(\beta_i') + \text{Var}(N) + 2 \cdot \text{Cov}(\beta_i', N) \tag{2}$$

Since the noise is a property of the instrument, it is reasonable to assume that it is uncorrelated with the flow; we can therefore set $\text{Cov}(\beta_i', N)$ to 0. Thus, the estimated variance from the beam
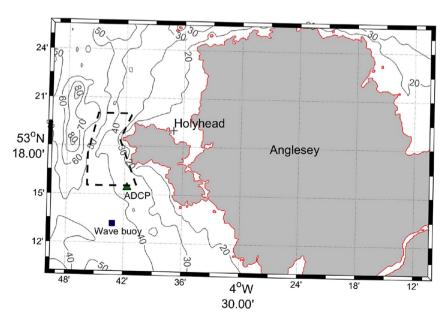

Fig. 1. Location of West Anglesey Demonstration Zone off the coast of Anglesey, marked with black dashed line. Bathymetry contours show depth relative to mean sea level.

measurements will have a positive bias relative to the true velocity variance, and our calculated value of TKE from equation (1) will be greater than it ought to be. Our dataset includes many measurements in still water, at which times the TKE will be negligibly small. Any non-zero TKE estimates at such times are therefore attributable to instrument noise, and we use the values of these estimates to quantify the TKE bias. In this way, we find that the TKE estimates have a positive bias of $9 \times 10^{-3} \text{J·kg}^{-1}$; all ADCP TKE estimates presented in this paper have been corrected to account for this bias.

2.1.2. Dissipation

Dissipation can be estimated using structure function analysis, a method based on spatially-separated velocity measurements. It was originally developed for use in atmosphere [33], but it has been shown to be applicable in a variety of marine conditions [23,34]. We start by defining the structure function $D(z,r)$ as the time-mean value of the squared velocity difference between two points separated by a distance r:

$$D(z,r) = \left\langle \left(b_i(z)' - b_i(z+r)' \right)^2 \right\rangle \tag{3}$$

On the condition that the maximum separation, r, is on the scale of the inertial subrange, the expected dependence of $D(z,r)$ on r is related to the dissipation:

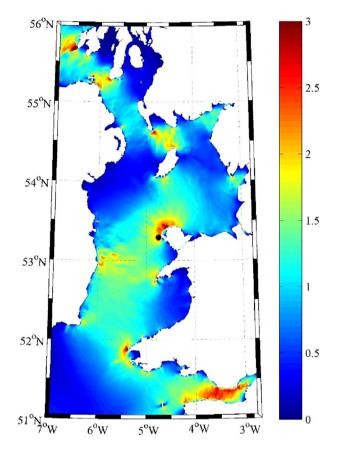$$D(z,r) = C_v^2 \varepsilon(z)^{2/3} r^{2/3} + N \tag{4}$$

Here N is an offset term that arises due to instrument noise and C_v is an empirically-determined constant; following Wiles et al. [23] and Mohrholz et al. [34], we take $C_v = 2.1$. It is then straightforward to carry out a least-squares fit of the calculated $D(z,r)$ values from equation (3) to the relation specified in 4, and from its slope get an estimate of ε. The maximum separation used for this fit is 5.1 m in the along-beam direction (i.e., 8 bins); we have confirmed that this separation lies within the inertial subrange by examination of the turbulent spectra.

2.2. Simulation of tidal flows using ROMS

The model domain, shown in Fig. 2, covers the area between 51°N and 56°N, and from 7°W to 2.7°W. It uses ten vertical layers (sigma coordinate system) evenly spaced throughout the water column and an orthogonal C-grid at $1/240°$ fixed longitudinal resolution (2012 × 1033 interior points, giving a grid spacing of approximately 300 m). Digitised Admiralty data, at 200 m horizontal resolution and corrected for mean sea-level variations [35], was interpolated to the computational grid, with a minimum water depth of 10 m. There was no wetting and drying as the geographic scale of inter-tidal regions was relatively small in relation to the model resolution and extent of the Irish Sea [15].

Our ROMS model has previously been successfully applied to Irish Sea tidal-stream resource analysis and is well validated [35], and so the model is described only briefly in this paper. A 91-day simulation was analysed; this covered the entire duration of the ADCP deployment and excluded two days before the start of the ADCP deployment to allow the model to spin up from an initial stationary state. The open boundary of the tidal model was forced with ten tidal constituents (M2, S2, N2, K2, K1, O1, P1, Q1, Mf, and Mm).

A drag coefficient $C_D = 0.003$ was assumed within the quadratic friction model parameterisation, which is consistent with previous ROMS studies of energetic tidal sites (e.g., Neill et al. [13]). Similar results have been found when comparing turbulence closure and

Fig. 2. Map of ROMS model domain. Contours show depth-averaged peak spring tidal current in ms^{-1}, as measured by the magnitude of the M2 and S2 components. Location of WADZ indicated by black circle near centre of the image.

GLS schemes in ROMS [16]. This is the reason for the choice of turbulence closure GLS model tuned to the $k - \varepsilon$ turbulence model, with standard parameters: p = 3, m = 1.5 and n = −1 (for further details see Warner et al. [16]).

Model validation is detailed in Lewis et al. [35] and is only summarised here. Results were compared with seven tide gauges from the National Tidal and Sea Level Facility (see www.ntslf.org), and the model was shown to have an 4% accuracy in simulating the amplitude of the major semi-diurnal lunar constituent, M2, (0.11 m RMSE), with M2 phase accurate to within 4°; for the major semi-diurnal solar constituent (S2) tidal height was simulated with 9% accuracy (0.08 m RMSE) and phase with 9° accuracy. Nine depth-averaged, and 131 depth-specific, M2 tidal current stations were used to validate simulated tidal currents, with a 10% velocity error and a 4°−7° phase error found.

3. Results

We first compare the measured and modelled mean flow properties. The principle semi-diurnal lunar (M2) tidal ellipse analysis of depth-mean tidal velocity data from the ADCP deployment compared to that simulated by our ROMS model gave a RMSE of 5% for C_{max} (the semi-major ellipse velocity component) and 0% C_{min} (the semi-minor ellipse velocity component). The inclination of the current ellipse error was 3° and phase error (degrees relative to Greenwich) was 6°: we are therefore satisfied that our model has accurately captured the mean flow dynamics at the measurement site.

3.1. Comparison of turbulence parameters — k and ε

Fig. 3 illustrates how mean TKE varies over the ADCP deployment period. This clearly shows that the ADCP measurements are strongly wave-dominated in the upper half of the water column. The lack of wave effects in the ROMS model means we cannot usefully compare TKE results in this depth range; for the lower half of the water column, however, the comparison becomes more meaningful, as shown in Fig. 4. Note that even when we examine only this deeper portion of the flow, we still see anomalous spikes (around 6th–7th October, 18th–22nd October and 6th–7th November). By cross-referencing to Fig. 3, we can see that these are periods of particularly strong wave activity, and we therefore surmise that these anomalies are due to wave action dominating the turbulent fluctuations even into the deepest part of the water column. These discrepancies are explored in more detail in Figs. 8 and 10.

The ability of ROMS to capture mean flow velocities is already well attested [13], and this is borne out by the results presented in the lower panel of Fig. 4. The upper panel depicts mean TKE values for the lower half of the water column. Note that what is meant by 'lower half of the water column' is not exactly the same for both ROMS and ADCP results. For the ADCP, this depth range is 1.89–19.29 m. This is obtained by taking the depth range halfway from the lowest bin up to the highest bin which yields useful data before sidelobe interference makes it impossible to obtain meaningful velocity measurements. This does not extend down to the seabed due to the ADCP's blanking distance, the ADCP itself and its support frame. ROMS discretises the water column into ten sigma layers, which correspond to different depths as the sea level changes over the tidal cycle. We use the lower five sigma layers for our estimate of column-mean TKE; this depth range always starts at the seabed but its maximum value ranges from 16.8 m to 18.8 m over the simulated period.

We can see that the agreement between ROMS and ADCP measurements is quite satisfactory. The spring-neap cycle is clearly apparent in the TKE data as a long-term modulation in magnitude, and when comparing the model predictions with the field data the size of this effect is very similar. More subtly, there is a flood-ebb asymmetry: TKE maxima tend to be higher on ebbs than floods. This can be seen in the time record subset shown in Fig. 5, where negative mean current speeds, corresponding to ebbs, coincide with higher-magnitude spikes in TKE density. The ROMS model also predicts this turbulence asymmetry (cf. the similar tidal asymmetry
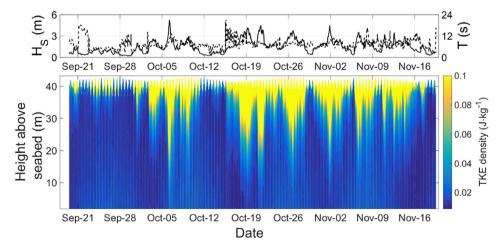
demonstrated in Ref. [13]), which, as shown in Fig. 6, is not due solely to differences in the mean flow: we see that TKE is consistently higher on ebbs than floods even when mean velocity magnitude is the same. Concomitantly, turbulence intensity is greater on ebbs than on floods, on average by 8% when looking at ROMS estimates or by 9% when looking at ADCP measurements.

Note that this asymmetry is not distributed evenly throughout the water column, as seen in Fig. 7. The differences between flood and ebb are more strongly pronounced mid-column, while near-bed depths show relatively little dependence on tidal phase. This depth dependence is seen in both simulations and measurements, although ROMS predicts significantly stronger asymmetry in mid-column than is observed in the ADCP data.

We can gain better insight into the comparison of model predictions and measured values by examining the statistics of the whole dataset as well as suitable subsets. In Fig. 8, we see that the scatter plots indicate a strong correspondence between model and measurements. For the mean velocity, there is a clear linear fit, with a RMSE of 0.20 ms^{-1} and an R^2 value of 0.98. We note, however, that the ROMS tends to overpredict mean velocity slightly when compared to measurements: the line of best fit has a slope of 1.11, rather than the value of 1 that would be found with perfect agreement.

The TKE agreement is less strong: the RMSE is 4.3×10^{-3} J·kg^{-1}, giving a scatter index of 0.41, and calculating a linear fit gives an R^2 value of 0.65. We can see that there is a tendency for ADCP measurements to exceed the corresponding ROMS predictions i.e., there are more points below the 1:1 line than above it, and they tend to lie further from the line of equality. As we discussed above, there are times when wave action dominates turbulent fluctuations even into the lower half of the water column. Measurements from these times are difficult to meaningfully compare with the ROMS predictions; we therefore examine whether the comparison improves when measurements taken at times of strong wave activity are excluded from consideration.

The criterion for exclusion is based on measurements taken by the wave buoy. We examine the range significant wave height (H_S) values observed from the wave buoy throughout the ADCP deployment, and define high-wave conditions as values of H_S in the 95th percentile. When these points are excluded, the RMSE of the TKE agreement drops to 3×10^{-3} J·kg^{-1} (scatter index 0.30) and the linear fit has an R^2 of 0.84. Applying a still stricter criterion that excludes measurements corresponding to H_S in the 75th percentile gives an RMSE of 2.3×10^{-3} J·kg^{-1}, a scatter index of 0.25 and a

Fig. 3. Lower panel shows TKE density as calculated in equation (1), upper panel shows simultaneously-collected wavebuoy data: significant wave height (H_S) as solid line, wave period (T) as solid line. Note that the range of TKE values is truncated at the upper end in order to make low-TKE features visible.
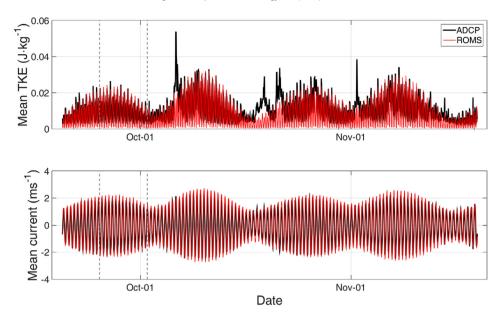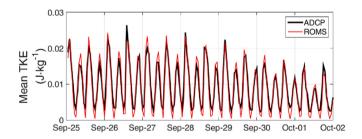
Fig. 4. Comparison of ADCP and ROMS results over the time period of the ADCP deployment. Upper panel shows time series of vertical-mean TKE from the lower half of the water column. Lower panel shows mean current velocities; flood velocities are shown as positive and ebb velocities as negative. Dashed grey lines indicate the subset shown in more detail in Fig. 5.

best-fit R^2 of 0.90.

Plotting the probability distribution functions (PDFs) of the mean TKE values (Fig. 9) allows us to compare the ROMS and ADCP data in a population sense. Note that in calculating these PDFs we have applied the 95th percentile condition on waves. We see that there is good agreement at the high-energy end of the PDFs, but less so at lower TKE values. Unsurprisingly, this means that when we divide the data points into slacks, ebbs and floods, the non-slack PDFs agree quite closely with one another but the slacks show a greater disparity.

We can also examine the comparative distributions of TKE between ROMS and ADCP results using q-q plots, as seen in Fig. 10. Visualising the results in this manner reinforces the conclusions we have drawn from studying the probability distributions themselves.
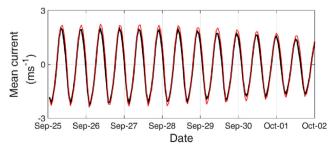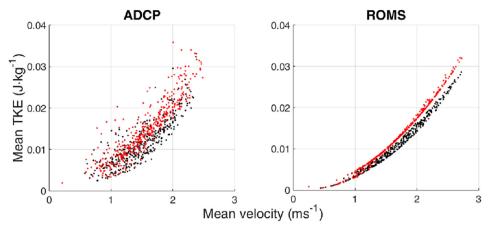

Fig. 5. Subset of the results from Fig. 4.

For low TKE values the ADCP measurements tend to be significantly higher than ROMS estimates, which is visible as the quantile points dipping below the equality line in the bottom left of the plots; we see this in the plot of all tides as well as in the floods and ebbs individually. At slack water, where TKE values are in general lower than when current speeds are high, all data points on the q-q curve lies below the line of equality.

In addition to the temporal variation and distribution of the TKE, we are interested in its vertical variation. Fig. 11 compares profiles of TKE density from the ROMS model and ADCP measurements. It also shows how the vertical profile from ADCP data varies depending on how strictly high-wave conditions are excluded from consideration. Obviously this has a more significant effect in the upper half of the water column: in this region, the 95th percentile profiles exceeded the 75th percentile profiles by 68% on the flood and 54% on the ebbs, whereas in the lower half the differences were only 9% and 4% respectively. The quantitative agreement between ROMS and ADCP is satisfactory for this deeper section: the ADCP data exceeds the ROMS prediction by 13% on ebbs and only 2% on floods.

The agreement in dissipation is less satisfactory. Fig. 12 shows comparisons of dissipation time series at four locations in the lower half of the water column. As we mention above, ROMS sigma layers and ADCP bins do not measure at exactly the same depths, but we have selected the closest depth matches from the available data. The time dependence tracks very closely: the correlation coefficient between ROMS and ADCP estimates of dissipation varies between 0.86 and 0.95 ($p < 0.001$) depending on depth. However, there is a significant discrepancy in magnitude, particularly closer to the seabed. ROMS estimates of dissipation exceed ADCP measurements by a factor of at least 1.5 on average for the highest location shown, and this factor rises to 4.8 for the location nearest the bed. Note that slacks were excluded in calculating this, as the measured values were very close to zero during slack water, leading to extremely high values of the ratio.

4. Discussion

We have found that the ROMS predictions of TKE match the

Fig. 6. Scatter plot comparing mean flow and TKE for ADCP measurements (left panel) and ROMS estimates (right panel). Black points correspond to flood phases, red points to ebb phases. (For interpretation of the references to colour in this figure legend, the reader is referred to the web version of this article.)
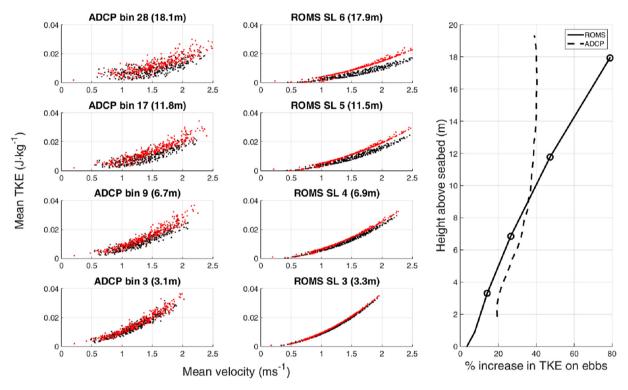

Fig. 7. Scatter plot comparing mean flow velocity and TKE at four depths for ADCP measurements (left column) and ROMS estimates (central column). Black points correspond to flood phases, red points to ebb phases. Right column shows a profile of flood-ebb asymmetry as a percentage increase in TKE density from flood to ebb. Circles indicate the depths from which the data in scatter plots are taken. (For interpretation of the references to colour in this figure legend, the reader is referred to the web version of this article.)
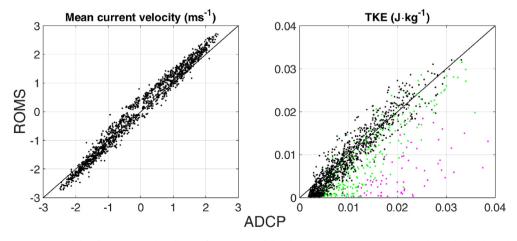

Fig. 8. Scatter plots comparing measured data from ADCP and predictions from ROMS. Left-hand panel shows mean current velocities; right-hand panel shows mean TKE for the lower half of the water column. In the TKE comparison, magenta points are excluded if the 95th %ile criterion for waves is applied; if the 75th %ile criterion is applied, the green points are also excluded. (For interpretation of the references to colour in this figure legend, the reader is referred to the web version of this article.)
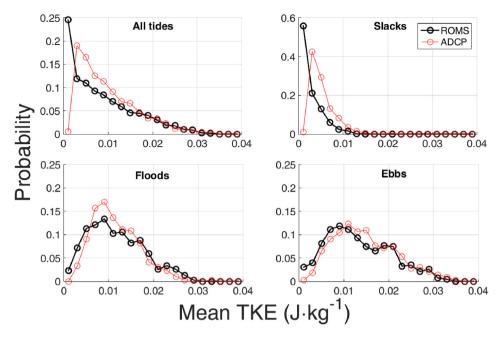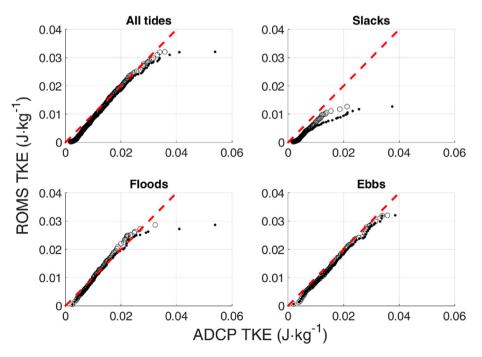
Fig. 9. Comparison of probability distributions of mean TKE for the lower half of the water column taken from ROMS simulation and ADCP data.

measured values well over the whole tidal cycle, although at times of relatively low turbulence the ADCP measurements are higher than the estimates produced by ROMS. This is visible in the low end of the probability distributions depicted in Fig. 9; we can also see it in the 'drooping tail' of the q-q plots in Fig. 10. We can conclude, then, that at these times either the measurements are erroneously high or the numerical predictions too low.
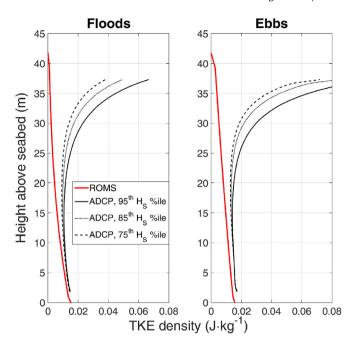
A systematic overestimation of TKE by the ADCPs would suggest that the measurements are biased high. However, as we discussed in section 2.1.1, it is well-known that the variance method of

calculating TKE from ADCP measurements will be positively-biased, and we have applied a correction for this. Furthermore, this correction is conservative in that it cannot undercorrect, only overcorrect. We can be sure of this because both the true value of TKE and its estimate obtained with variance method are always positive, and we calculate the bias by taking the smallest estimated value of TKE prior to applying the correction. If the bias were any greater than this, the lowest uncorrected estimate of TKE would correspond to a true TKE of less than zero, which is impossible.

This suggests that the discrepancy must be due to an

Fig. 10. Comparison of TKE probability distributions between ROMS simulation and ADCP measurements visualised as q-q plots. Dots show the quantiles for the complete data set, circles show quantiles for the data set with the 95th %ile condition on waves applied; the line of equality is shown as red dashes. To improve legibility, only every fifth quantile has been plotted. (For interpretation of the references to colour in this figure legend, the reader is referred to the web version of this article.)

Fig. 11. Vertical profiles of TKE density for ROMS results and ADCP data. Different ADCP profiles correspond to different wave conditions. The 95th %ile wave ADCP profile uses only data from times during which H_S did not exceed the 95th percentile to calculate the mean; a similar condition applies for the 85th %ile and 75th %ile profiles.
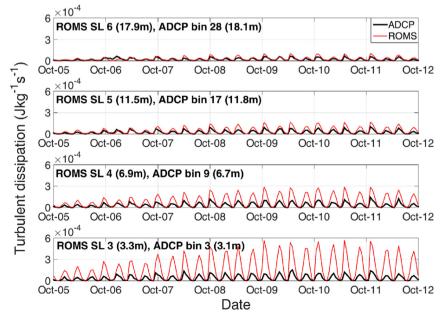
underestimate of TKE in the numerical model. However, recall that with the variance method it is not possible to distinguish between fluctuations due to turbulence and due to other sources, as is clearly illustrated by the dominance of wave effects seen in the vertical profiles of TKE (Fig. 11). The TKE represented by k in the turbulence closure scheme of the ROMS model reflects the turbulent energy contained in the fluctuations in the classical wavenumber range [17]. An alternative explanation for the difference might then be

that the measured values of TKE are including the effects of fluctuations excluded from the ROMS turbulence model, such as velocity variations on lengthscales intermediate between the mean flow and classical turbulence, or wave action. The difference in TKE between ADCP and ROMS at times of low turbulence, as shown in Fig. 13, is fairly well-correlated with wave height ($R = 0.725$, $p < 0.001$), lending support to this as at least a partial explanation.
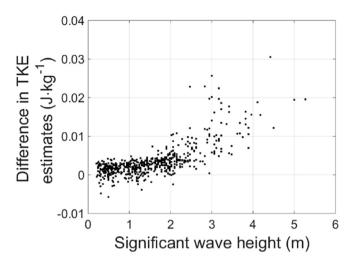
The importance of wave effects is one of the most striking observations from ADCP data. Previous studies of turbulence at energetic tidal sites based on ADCP measurements [17,29] did not indicate such strong influence by waves, but these were in more sheltered bodies of water with much shorter fetch and consequently less energetic waves. In the current study, wave effects dominated turbulence throughout much of the water column, to the extent that some methods of analysing ADCP data cannot be applied: specifically, spectral analysis for estimation of turbulent dissipation.

Spectral analysis is a well-known technique for determining the turbulent dissipation [24,27], based on Kolmogorov's theory of the inertial subrange which asserts that, for some range of frequencies (or wavenumbers), the power spectral density (PSD) of turbulent velocity fluctuations will exhibit a $-5/3$ power-law dependence on frequency. In this subrange, the PSD is a function only of the frequency and the turbulent dissipation rate, ε. Thus, by fitting the spectrum to the expected slope, it is possible to obtain an estimate of ε. However, as can be seen in Fig. 14, there is a large, broad peak in the middle of the expected inertial subrange. This peak coincides with the median wave period during the ADCP deployment: it is reasonable to conclude that this corresponds to wave activity during the measurement period. Note that Doppler noise begins to dominate the spectrum as we approach the Nyquist frequency of 1 Hz, so it is not possible to perform a fit in this part of the spectrum.

It may be possible to filter out the wave effects, either in a simple bandpass sense or by applying a more sophisticated model of the wave spectrum based on the significant wave height and period measured by the wave buoy. However, we should remember that the fundamental motivation of this study of turbulence is to predict

Fig. 12. Comparison of time series of dissipation at four locations in water column from ROMS (red) and ADCP (black) for representative time period. SL denotes the sigma layer number from the ROMS simulation. Note the vertical scale differs for the lowest panel. (For interpretation of the references to colour in this figure legend, the reader is referred to the web version of this article.)
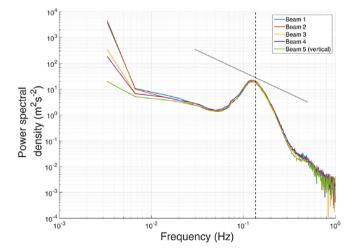
Fig. 13. Scatter plot visualising the effect of wave height as measured by buoy on difference in TKE density from ADCP measurements and ROMS estimates.

its effects on the fatigue life and reliability of TEC components. The source of a fluctuating load in this context is immaterial; it is the characteristics (i.e., magnitude and period) of the load itself that are most important. In this case, separating out the wave and turbulent fluctuations provides no meaningful benefit.

If this is the case, the observations presented in this paper suggest that, for TEC deployment sites that are not sheltered from waves, the effects of waves on fatigue load will be of much greater concern than the effects of turbulence in the marine currents. This is obviously dependent on the location of the TEC within the water column: seabed-mounted devices that are small relative to the total water depth will be more sensitive to the turbulence in the tidal currents, but larger devices, and floating or semi-submersible designs of all sizes, will be far more affected by wave action.

Earlier work on validating the turbulence models of ROMS for highly-energetic tidal sites [17] found that dissipation was well-matched between predictions and measurements, while turbulent kinetic energy was not captured as satisfactorily. Differences in TKE were attributed to the limited lengthscales represented by k in

Fig. 14. Mean power spectral densities across the whole ADCP record for each of the five beams; each coloured line corresponds to a different beam. Grey line shows the expected −5/3 slope, and dotted black line shows the median wave period during the ADCP deployment. (For interpretation of the references to colour in this figure legend, the reader is referred to the web version of this article.)

the turbulence closure model; correcting the ROMS estimates based on this assumption led to a much better agreement.

The work we present here, however, finds that ROMS estimates of TKE are very well corroborated by the measured values, and no similar correction term is required. Dissipation, on the other hand, is found to differ significantly between model and measurements. It is not clear why this is. The structure function method is being applied in an appropriate manner: based on spectral analysis, the separation distances used in its calculation lie within the inertial subrange, and the fits to the expected $2/3$ slope are satisfactory. If instead the problem lies with ROMS overestimating dissipation, then we would also expect that the turbulent production should be much greater, but there is no indication that this is the case.

5. Conclusions

We have found that ROMS estimates of turbulence, as measured by TKE, agree very well with ADCP measurements at a site with strong tidal currents across two complete spring-neap cycles. There are a few caveats to this observation. Firstly, wave action largely drowns out turbulent fluctuations in the upper half of the water column when analysing the measured data, and for particularly high waves this effect extends deeper still. Secondly, the measured TKE values show a consistent level of background turbulence at times of slow flow, even when corrected for positive bias, that is not captured by the ROMS model. Lastly, although TKE estimates match measurements very well, turbulent dissipation shows far weaker agreement. Nonetheless, this study demonstrate that ROMS is a suitable tool for predicting the strength of turbulence at the types of highly-energetic site typically chosen for TEC deployment.

References

[1] P.L. Fraenkel, Power from marine currents, Proc. Inst Mech. Eng. Part A J. Power Energy 216 (1) (2002) 1—14.
[2] W.M.J. Batten, A.S. Bahaj, A.F. Molland, J.R. Chaplin, The prediction of the hydrodynamic performance of marine current turbines, Renew. Energy 33 (5) (2008) 1085—1096.
[3] M. Willis, I. Masters, S. Thomas, R. Gallie, J. Loman, A. Cook, R. Ahmadian, R. Falconer, B. Lin, G. Gao, et al., Tidal turbine deployment in the Bristol Channel: a case study, Proc. ICE Energy 163 (3) (2010) 93—105.
[4] F. Maganga, G. Germain, J. King, G. Pinon, E. Rivoalen, Experimental characterisation of flow effects on marine current turbine behaviour and on its wake properties, IET Renew. Power Gener. 4 (6) (2010) 498.
[5] D.V. Val, L. Chernin, D.V. Yurchenko, Reliability analysis of rotor blades of tidal stream turbines, Reliab. Eng. Syst. Saf. 121 (2014) 26—33.
[6] J.H. Simpson, H. Burchard, N.R. Fisher, T.P. Rippeth, The semi-diurnal cycle of dissipation in a ROFI: model-measurement comparisons, Cont. Shelf Res. 22 (11) (2002) 1615—1628.
[7] H. Burchard, P.D. Craig, J.R. Gemmrich, H. van Haren, P.-P. Mathieu, H.M. Meier, W.A.M.N. Smith, H. Prandke, T.P. Rippeth, E.D. Skyllingstad, et al., Observational and numerical modeling methods for quantifying coastal ocean turbulence and mixing, Prog. Oceanogr. 76 (4) (2008) 399—442.
[8] M. Edmunds, R. Malki, A. Williams, I. Masters, T. Croft, Aspects of tidal stream turbine modelling in the natural environment using a coupled bem—cfd model, Int. J. Mar. Energy 7 (2014) 20—42.

[9] I. Masters, A. Williams, T.N. Croft, M. Togneri, M. Edmunds, E. Zangiabadi, I. Fairley, H. Karunarathna, A comparison of numerical modelling techniques for tidal stream turbine analysis, Energies 8 (8) (2015) 7833–7853.

[10] A. Shchepetkin, J. McWilliams, Regional ocean model system: a split-explicit ocean model with a freesurface and topography-following vertical coordinate, Ocean. Model. 9 (2005) 347–404.

[11] D.B. Haidvogel, H. Arango, W.P. Budgell, B.D. Cornuelle, E. Curchitser, E. Di Lorenzo, K. Fennel, W.R. Geyer, A.J. Hermann, L. Lanerolle, et al., Ocean forecasting in terrain-following coordinates: formulation and skill assessment of the regional ocean modeling system, J. Comput. Phys. 227 (7) (2008) 3595–3624.

[12] J.C. Warner, C.R. Sherwood, R.P. Signell, C.K. Harris, H.G. Arango, Development of a three-dimensional, regional, coupled wave, current, and sediment-transport model, Comput. Geosci. 34 (10) (2008) 1284–1306.

[13] S.P. Neill, M.R. Hashemi, M.J. Lewis, The role of tidal asymmetry in characterizing the tidal energy resource of Orkney, Renew. Energy 68 (2014) 337–350.

[14] S.P. Neill, M.R. Hashemi, M.J. Lewis, Optimal phasing of the european tidal stream resource using the greedy algorithm with penalty function, Energy 73 (2014) 997–1006.

[15] M. Lewis, S. Neill, M. Hashemi, M. Reza, Realistic wave conditions and their influence on quantifying the tidal stream energy resource, Appl. Energy 136 (2014) 495–508.

[16] J.C. Warner, C.R. Sherwood, H.G. Arango, R.P. Signell, Performance of four turbulence closure models implemented using a generic length scale method, Ocean. Model. 8 (1) (2005) 81–113.

[17] K.M. Thyng, J.J. Riley, J. Thomson, Inference of turbulence parameters from a ROMS simulation using the k-ε closure scheme, Ocean. Model. 72 (2013) 104–118.

[18] F. Rowe, J. Young, An ocean current profiler using doppler sonar, in: OCEANS'79, IEEE, 1979, pp. 292–297.

[19] K. Theriault, Incoherent multibeam Doppler current profiler performance: Part I–Estimate variance, IEEE J. Ocean. Eng. 11 (1) (1986) 7–15.

[20] Y. Lu, R.G. Lueck, Using a broadband ADCP in a tidal channel. Part I: mean flow and shear, J. Atmos. Ocean. Technol. 16 (11) (1999) 1556–1567.

[21] A. Lohrmann, B. Hackett, L.P. Rø, High resolution measurements of turbulence, velocity and stress using a pulse-to-pulse coherent sonar, J. Atmos. Ocean. Technol. 7 (1) (1990) 19–37.

[22] Y. Lu, R.G. Lueck, Using a broadband ADCP in a tidal channel. Part II: Turbulence, J. Atmos. Ocean. Technol. 16 (11) (1999) 1568–1579.

[23] P.J. Wiles, T.P. Rippeth, J.H. Simpson, P.J. Hendricks, A novel technique for measuring the rate of turbulent dissipation in the marine environment, Geophys. Res. Lett. 33 (21) (2006) 1–5.

[24] J.M. McMillan, A.E. Hay, R.G. Lueck, F. Wolk, Rates of dissipation of turbulent kinetic energy in a high Reynolds Number tidal channel, J. Atmos. Ocean. Technol. 33 (4) (2016) 817–837.

[25] M.T. Stacey, S.G. Monismith, J.R. Burau, Measurements of Reynolds stress profiles in unstratified tidal flow, J. Geophys. Res. Oceans. (1978–2012) 104 (C5) (1999) 10933–10949.

[26] E.A. Nystrom, C.R. Rehmann, K.A. Oberg, Evaluation of mean velocity and turbulence measurements with ADCPs, J. Hydraulic Eng. 133 (12) (2007) 1310–1318.

[27] E. Osalusi, J. Side, R. Harris, Structure of turbulent flow in EMEC's tidal energy test site, Int. Commun. Heat Mass Transf. 36 (5) (2009) 422–431.

[28] M. Togneri, I. Masters, Comparison of turbulence characteristics for some selected tidal stream power extraction sites, in: Proceedings of the 9th Conference on Engineering Turbulence Modelling and Measurements, 2012.

[29] M. Togneri, I. Masters, Micrositing variability and mean flow scaling for marine turbulence in Ramsey Sound, J. Ocean Eng. Mar. Energy 2 (1) (2016) 35–46.

[30] J. Thomson, B. Polagye, V. Durgesh, M.C. Richmond, Measurements of turbulence at two tidal energy sites in Puget Sound, WA, Ocean. Eng. IEEE J. 37 (3) (2012) 363–374.

[31] T.P. Rippeth, J.H. Simpson, E. Williams, M.E. Inall, Measurement of the rates of production and dissipation of turbulent kinetic energy in an energetic tidal flow: red wharf bay revisited, J. Phys. Oceanogr. 33 (9) (2003) 1889–1901.

[32] I. Nezu, H. Nakagawa, Turbulence in Open-channel Flows, Taylor & Francis, 1993.

[33] H. Sauvageot, Radar Meteorology, Artech House Publishers, 1992.

[34] V. Mohrholz, H. Prandke, H. Lass, Estimation of TKE dissipation rates in dense bottom plumes using a Pulse Coherent Acoustic Doppler Profiler (PC-ADP) Structure function approach, J. Mar. Syst. 70 (3) (2008) 217–239.

[35] M. Lewis, S. Neill, P. Robins, M. Hashemi, Resource assessment for future generations of tidal-stream energy arrays, Energy 83 (2015) 403–415.